THE ROYAL SOCIETY

Published online 29 December 2004

A model of stereocilia adaptation based on single molecule mechanical studies of myosin I

Christopher Batters[1], Mark I. Wallace[1], Lynne M. Coluccio[2] and Justin E. Molloy[1*]

[1]*Division of Physical Biochemistry, MRC National Institute for Medical Research, The Ridgeway, Mill Hill, London NW7 1AA, UK*

[2]*Boston Biomedical Research Institute, 64 Grove Street, Watertown, MA 02472, USA*

We have used an optical tweezers-based apparatus to perform single molecule mechanical experiments using the unconventional myosins, Myo1b and Myo1c. The single-headed nature and slow ATPase kinetics of these myosins make them ideal for detailed studies of the molecular mechanism of force generation by acto-myosin. Myo1c exhibits several features that have not been seen using fast skeletal muscle myosin II. (i) The working stroke occurs in two, distinct phases, producing an initial 3 nm and then a further 1.5 nm of movement. (ii) Two types of binding interaction were observed: short-lived ATP-independent binding events that produced no movement and longer-lived, ATP-dependent events that produced a full working stroke. The stiffness of both types of interaction was similar. (iii) In a new type of experiment, using feedback to apply controlled displacements to a single acto-myosin cross-bridge, we found abrupt changes in force during attachment of the acto-Myo1b cross-bridge, a result that is consistent with the classical 'T_2' behaviour of single muscle fibres. Given that these myosins might exhibit the classical T_2 behaviour, we propose a new model to explain the slow phase of sensory adaptation of the hair cells of the inner ear.

Keywords: optical tweezers; molecular motors; Myo1c; hearing; sensory adaptation

1. INTRODUCTION

The vertebrate sensory organs of hearing and balance work by converting minute mechanical forces produced by sound waves and mechanical vibrations into nerve impulses. The sensory hair cells of the cochlea and vestibular system have highly ordered bundles of stereocilia that project from the cell surface into the fluid-filled chambers of the inner ear. Small deflections of the bundle tip cause shearing between adjacent stereocilia that is sensed by a stiff proteinaceous tip-link filament (Siemens *et al.* 2004; Sollner *et al.* 2004) that pulls on a mechanically gated ion channel (see figure 1*a*). The physiological amount of displacement is a few nanometres and the forces are a few piconewtons. Hair cells are exquisitely sensitive to rapidly changing signals, but exhibit sensory adaptation, i.e. their output rapidly accommodates to steady-state signals. Sensory adaptation is a general phenomenon: you respond immediately to a mosquito landing on your neck and yet are unaware that you are wearing clothes.

Sensory physiologists have performed extensive studies using intact, single hair cells isolated from turtle, frog and mouse cochlear and vestibular systems. These studies have shown that direct mechanical gating of ion channels at the tips of the stereocilia leads to depolarization of the hair cell membrane and in turn to neuronal output (Corey & Hudspeth 1983; Glowatzki & Fuchs 2002). Tension in the tip-link filaments causes channels to open or close and the resulting motions of the ion channel gate contribute compliance in the stereocilia bundle (Howard & Hudspeth 1988). Analysis of rapid step changes in bundle position reveals a non-linear force–extension diagram with an inflection (i.e. dip in stiffness) at around the same set position that gives the steepest change in channel open probability. The inflection in the force–extension diagram resembles the so-called 'T_2' curve measured for single muscle fibres (Huxley & Simmons 1971). However, unlike the tension changes observed with muscle fibres (which occur on a millisecond timescale), the relaxation process due to channel opening or closing occurs on a microsecond timescale that is too fast to measure (Howard & Hudspeth 1988). In addition to tension changes due to channel opening there is the process of sensory adaptation during which channel re-closure occurs. This takes place on a much slower time-scale (ms) and coincides with a measurable relaxation in force. Adaptation is thought to be due to repositioning of the ion channels by an acto-myosin motor system (Holt & Corey 2000). At rest, the ion channels have an open probability of $p \approx 0.1$ and upon stimulation (termed a 'negative deflection' of the hair bundle) this increases to $p \approx 1$. This leads to slipping adaptation that acts to restore the open probability to $p \approx 0.1$. However, the adaptation process also occurs in response to positive bundle deflections known as climbing adaptation. We know that

* Author for correspondence (jmolloy@nimr.mrc.ac.uk).

One contribution of 14 to a Discussion Meeting Issue 'Myosin, muscle and motility'.

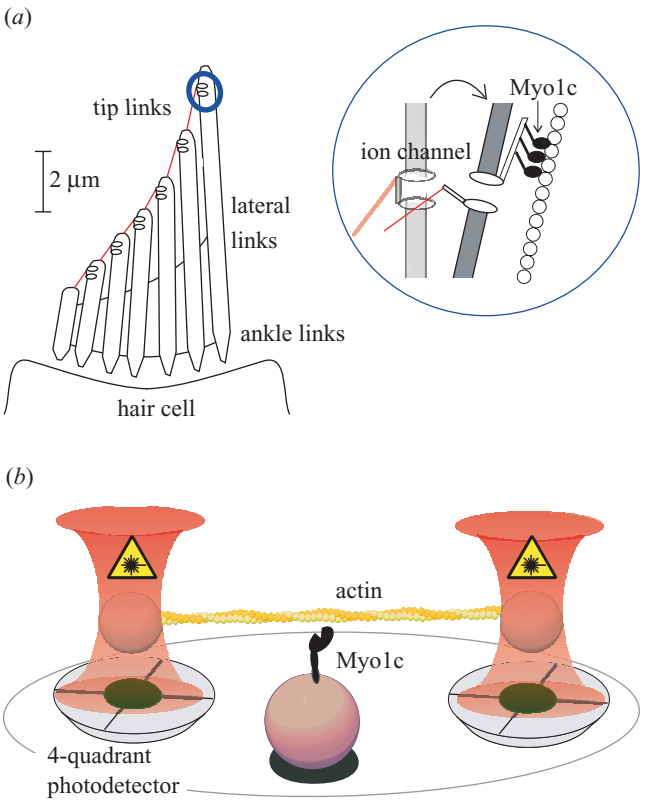

Figure 1. Hair cell structure and optical tweezers single molecule technique. (*a*) Each hair cell bundle consists of approximately 50 individual stereocilia each of which is *ca* 200 nm in diameter and *ca* 10 μm long (Jacobs & Hudspeth 1990). The stereocilia consist of a core bundle of actin filaments and a surrounding plasma membrane that is contiguous with the rest of the hair cell membrane. The connecting filament or 'tip link', which is probably very stiff, was recently shown to be cadherin 23 (Siemens *et al.* 2004; Sollner *et al.* 2004). Most of the compliance in the system comes from bending about the base of the stereocilia and movements of the ion channels themselves (inset). (*b*) Cartoon showing the three-bead geometry used for optical trapping experiments. The actin filament binds to the NEM-treated beads held in the optical tweezers. This is brought into the vicinity of a surface-bound myosin and binding events are monitored using the four-quadrant detectors.

actin filaments are oriented with their barbed (or 'plus') ends towards the bundle tip and myosin I is probably a 'plus end' directed motor, so climbing adaptation can be explained by forward cross-bridge cycling whereas slipping adaptation requires myosin to move backwards or to slip along actin.

The adaptation process in turtle vestibular hair cells requires two characteristic time constants in order to fit the relaxation in transduction current (Wu *et al.* 1999). It was suggested that the fast phase (0.3–5 ms) is caused by Ca^{2+} binding at a site 20–50 nm from the site of Ca^{2+} entry at the ion channel whilst the slow phase (10–100 ms) corresponds to an adaptation process perhaps involving an acto-myosin based motor (Holt & Corey 2000). Myo1c (Gillespie *et al.* 2001) is implicated in this sensory adaptation process (Howard & Hudspeth 1987) and its role has been confirmed convincingly by a recent series of experiments (Garcia *et al.* 1998; Gillespie *et al.* 1993; Holt *et al.* 2002). In the study of Holt *et al.* (2002) tyrosine-61 of Myo1c was mutated to glycine making it susceptible to inhibition by N^6-modified ADP analogues. The mutant Myo1c was expressed in transgenic mice. Addition of the ADP analogue to isolated hair cells from the mutant mice blocked adaptation to positive deflection. The speed and specificity of inhibition confirm that Myo1c has an integral role in adaptation. However, one should note that there is also good evidence for the involvement of another unconventional myosin, Myo7a, in the adaptation process (Weil *et al.* 1995; Kros *et al.* 2002) so the situation may, in fact, be more complex. For a more detailed review of the role of Myo1c in the inner ear, see Gillespie (2004). There is also evidence that Myo1c is involved in the translocation of GLUT4 glucose transporters in adipocytes (Bose *et al.* 2002) and maintenance of tension in neuronal cells (Diefenbach *et al.* 2002). Like Myo1c, the class I myosin, Myo1b, is ubiquitously expressed. Studies indicate that Myo1b is associated with several subcellular compartments (Ruppert *et al.* 1993; Balish *et al.* 1999) and might be involved in membrane trafficking (Cordonnier *et al.* 2001).

In the present study, we have used both Myo1b and Myo1c purified from rat liver (Coluccio & Conaty 1993), as this source gives sufficient quantities of purified protein required for our experiments. The ATPase activity of these myosins is slow (Coluccio & Geeves 1999; Batters *et al.* 2004) allowing us to investigate aspects of the acto-myosin interaction that are otherwise difficult to study using conventional, skeletal muscle myosin II.

The mechanical properties of acto-Myo1c interactions vary over a wide range of timescales. ADP also affects these mechanical properties over a similar timescale. In an earlier study, we found that ADP has a profound effect on the conformation of the acto-Myo1c complex and also its biochemical kinetics (Batters *et al.* 2004). We also examined the effect of Ca^{2+} on the interaction of actin with Myo1c because Ca^{2+} has profound effects on the adaptation process (Wu *et al.* 1999) and on the mechanical properties of stereocilia (Marquis & Hudspeth 1997). From solution biochemical studies it is clear that the ATPase, *in vitro* motility (Batters *et al.* 2004) and lipid binding (Tang *et al.* 2002) of Myo1c are also strongly dependent upon Ca^{2+}. The effects of calcium are not dealt with in the current paper.

2. THE OPTICAL TWEEZERS TECHNIQUE

The mechanical properties of single acto-myosin I (Myo1c and Myo1b) interactions were measured with an optical tweezer-based mechanical transducer using the three-bead geometry originally devised by Finer *et al.* (1994; figure 1*b*). Proteins (Myo1c, Myo1b and rhodamine–phalloidin labelled actin) were purified as described previously (Pardee & Spudich 1982; Kron & Spudich 1986; Coluccio & Conaty 1993). Myo1c and Myo1b were diluted to 4 μg ml^{-1} in a buffered salt solution (AB^- containing 25 μM KCl, 25 μM imidazole, 4 μM $MgCl_2$, 1 μM EGTA, pH 7.4, 22 °C) (Kron & Spudich 1986) and allowed to bind to a microscope coverslip. The surface was then blocked by flushing with 100 μl of AB^-/BSA (5 mg ml^{-1}). After blocking, the solution was replaced with AB^+/CP (AB^- supplemented with 2 μM creatine phosphate, 20 μM dithiothreitol (DTT),

various [ATP], 1 mg ml^{-1} creatine phosphokinase, 0.5 mg ml^{-1} BSA, 3 mg ml^{-1} glucose, 0.1 mg ml^{-1} glucose oxidase, 0.02 mg ml^{-1} catalase; Kishino & Yanagida (1988)). This solution also contained rhodamine–phalloidin-labelled actin filaments (see above) and 1.1 μm polystyrene beads (Sigma), which were pre-coated with NEM-modified myosin (Veigel *et al.* 1998). Experiments were performed at 23 °C. Laser optical tweezers were used to capture a single actin filament held between two NEM-myosin coated polystyrene beads. The filament was held in mid-solution, in the vicinity of a third, myosin-coated, surface-attached bead. Interactions between the suspended actin filament and surface bound myosin molecules were measured at optical tweezer stiffnesses (κ_{trap}) between 0.02 and 0.04 pN nm^{-1}. The motions of both optically trapped beads were monitored by bright-field microscopy. The defocused image of the two optically trapped beads produced dark spots on a white background. These images were cast onto two, four-quadrant photodetectors that gave a signal proportional to the centre of gravity of the bead image position (Molloy *et al.* 1995). Data were collected (at 2 kHz sampling frequency) while a 100 nm amplitude sine-wave (100 Hz) oscillation was applied to one of the laser traps. System stiffness was monitored from changes in pick-up of the sine-wave motion by the other bead and this was used as a sensitive monitor of system stiffness. This allowed short-lived acto-myosin binding events to be identified above the background thermal vibration. In order to probe the 'T_2' behaviour (e.g. movement of an actin-attached cross-bridge) we employed a position feedback loop. This allowed us to move the bead pair in a controlled manner through a triangular waveform displacement of 25 nm peak-to-peak amplitude and a frequency of 1 Hz. The servo-control signal used to drive the laser positions was recorded simultaneously with the bead positions so that we could later plot force–extension diagrams during the cross-bridge attached and unattached intervals of the records.

We performed a variety of mechanical experiments in order to explore the following phenomena:

(i) size and timing of the working stroke;
(ii) strain dependence of bound lifetimes;
(iii) Huxley–Simmons T_2 transients.

We first measured the time-course of acto-myosin cross-bridge interactions looking specifically for short-lived, weak-binding, interactions between actin and Myo1c. We also monitored the time-course of the production of movement during individual binding events to see if movement was produced in different phases. We then measured the strain dependence of the Myo1c cross-bridge lifetimes. Finally, we measured the force–extension response of single acto-Myo1b cross-bridges to explore their T_2 behaviour (Huxley & Simmons 1971). In this new type of experiment we used Myo1b because its working stroke is significantly larger and it is much easier to work with than Myo1c.

(a) *Time-course of acto-Myo1c mechanical interactions*

Interactions between a single, surface attached, Myo1c molecule and a single actin filament that was held using the optical tweezer arrangement were monitored (figure 1*b*). Intermittent changes in the noise of the records correspond to individual binding events (see figure 2*a*,*b*). The events started and ended abruptly and the duration of bound periods was stochastic and depended in a first order manner on the concentration of ATP in the bathing solution. Individual events were selected from the rather noisy records by analysis of the discrete Fourier transform of the data at the optical tweezer oscillation frequency (see figure 2 legend). Both the duration and amplitude of each individual binding event were measured from the original (untransformed) position data and further analysis was performed on that isolated data.

(b) *Analysis of the acto-Myo1c bound lifetimes*

Data were collected from several actin filaments and pooled to give a total set of over 800 individual binding events. The characteristic lifetime of the acto-Myo1c binding events (e.g. governed by the off-rate) was determined from a plot of the cumulative lifetime distribution (figure 2*c*). Casual inspection of the raw datasets revealed an excessive number of short-lived events (figure 2*a*, black arrows). These short-lived events had a similar stiffness to the longer-lived events (figure 2, grey arrows). Cumulative lifetime distribution plots were distinctly biphasic exhibiting a fast phase (representing *ca* 80% of the total counts) and a slow phase making up the remainder (figure 2*c*).

A double exponential decay was fitted to the data giving two rate constants and corresponding amplitudes. The experiment was performed at four ATP concentrations and the rate constants derived from the lifetime analysis were plotted as a function of ATP concentration (figure 2*d*). The fast phase (short-lived events) is independent of ATP and is *ca* 10 s^{-1}. The slow phase is ATP-dependent showing approximately Michaelis–Menten behaviour with a second order rate constant for ATP binding of 0.05 μM^{-1} s^{-1}, k_m of 18 μM and V_{max} of 1.7 s^{-1}. At this point we note that our earlier published work on Myo1c (Batters *et al.* 2004) showed that if binding events were ranked on the basis of their bound lifetimes then the local average movement produced depended in a characteristic fashion upon the lifetime. Short-lived events produced virtually no movement; longer-lived events produced a movement of *ca* 4.2 nm.

(i) *Summary*

We find that there is a significant population (80% of the total observations) of mechanically-stiff, short-lived binding events, whose lifetime is independent of ATP concentration and which produce no net movement when bound to actin.

(c) *The size of the Myo1c working-stroke*

The working-stroke produced by Myo1c was determined from a histogram of binding event displacement amplitudes (figure 3). The data show a large dispersion due to the background thermal vibration and superimposed sinusoidal perturbation. This is moderately well fitted by a Gaussian distribution with standard deviation of 12 nm $= (k_B T/\kappa)^{0.5}$, where $k_B T$ is the thermal energy of 4 pN nm, κ is the tweezer stiffness of 0.03 pN nm^{-1}. The histogram of binding events was shifted from the mean rest position by 3.4 ± 0.42 nm (s.e.m). We define this movement as the myosin working stroke. A small correction (+10%) was made to the raw data to account for

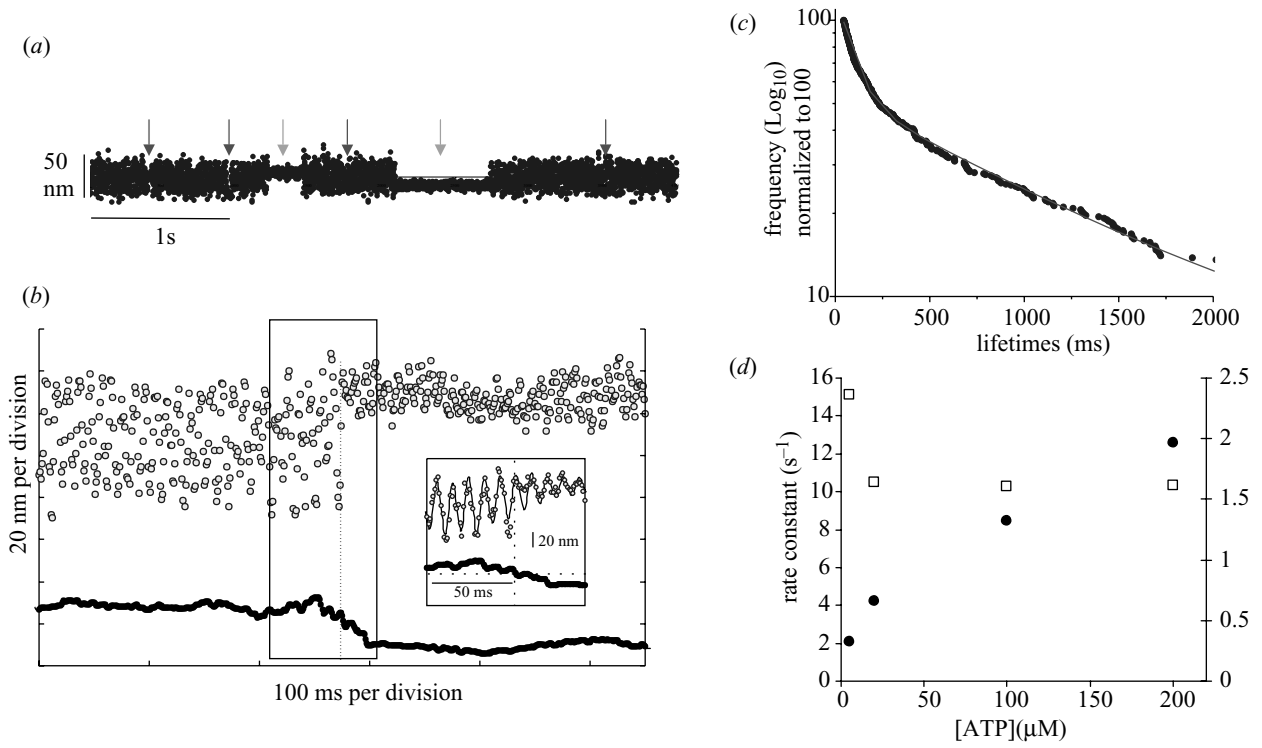

Figure 2. Analysis of single molecule mechanical recordings obtained from Myo1c. (*a*) A sample data trace showing acto-myosin binding events. The black arrows highlight the superfluity of short-lived events. The light arrows highlight the longer-lived population. The trace represents 4 s of data collected at 2 kHz sampling frequency (Myo1c, 23 °C, 20 μM ATP). (*b*) Open circles show some of the original data from (*a*) on an expanded timescale. The lower plot is the discrete Fourier transform of the data at the optical tweezer oscillation frequency (ω). The complex amplitude, A_c, of the signal, A, at each time point, t, was calculated as $A_c = [A\sin^2(\omega t)+A\cos^2(\omega t)]^{0.5}$ and the transformed data were smoothed (using a 50-point running average) and plotted (filled circles, lower trace). The start and end of each binding event was determined from the time-point at which a characteristic reduction (approximately fivefold) in amplitude of A_c occurred (inset). We employed a Schmitt trigger software algorithm to prevent false triggering due to noise around the threshold value. (*c*) A log-linear plot of the distribution of Myo1c lifetimes at 20 μM [ATP] ($n = 427$) (replotted from Batters *et al.* 2004) with a dual exponential decay fitted to the data $R^2 = 0.98$. (*d*) Effect of [ATP] on lifetime distributions. The fast lifetimes (open squares) do not show dependence on [ATP]; however, the slow phase (filled circles) shows Michaelis–Menten dependence of unbinding rate upon the [ATP] (see § 2b).

series compliance. This was measured from the ratio of bound and detached stiffnesses (Veigel *et al.* 1998).

To test whether Myo1c produces its working stroke in two separate phases, as seen with other myosin I types (Myo1b and brush border myosin I; (Veigel *et al.* 1999), an ensemble analysis was performed. Briefly, individual events were synchronized to the start and end of each interaction based on the change in system stiffness (see § 2a) and averaged to give an ensemble response (Veigel *et al.* 1999). We found that Myo1c exhibits a two-phase working stroke (data not shown). The amplitude of the first phase is 3.1 nm; and the second phase produces an additional working stroke of 1.1 nm, giving an overall displacement of 4.2 nm, s.d. 1.4 nm ($n = 85$). This finding was recently published elsewhere (Batters *et al.* 2004). Note that the total working stroke as measured by Batters *et al.* (2004) was larger than the 3.4 nm derived from the histogram method (see § 2c), which relies on simple averaging of each entire event (i.e. the two phases are combined and therefore the overall mean is lower than the peak displacement).

(d) *The effect of strain on the acto-Myo1c attached lifetime*

We analysed the single molecule binding events to investigate whether the acto-Myo1c bound lifetime depends upon load. To do this we exploited the fact that each binding event occurred at a random starting position relative to the centre of the optical tweezer and hence each experienced a random load. The average load, F, experienced during a given binding event is the product of the displacement of the beads from the tweezer centre, d, and the tweezer stiffness, κ (i.e. $F = \kappa d$; see figure 4). Binding durations and forces were ranked on the basis of the average force experienced during each event. Then, a 40-point running mean average was applied to both lifetime and force data. This gave a table of data consisting of average lifetimes and corresponding average forces. The reciprocal lifetime (i.e. the apparent unbinding rate constant) was then plotted as a function of force. We found that relatively small forces (from −1 to +1 pN) have quite a strong effect on the cross-bridge unbinding rate. When a cross-bridge is pushed in the direction of its working stroke (negative load) its detachment rate is faster than when it is pulled against the direction of its working stroke (positive load).

3. APPLICATION OF CONTROLLED DISPLACEMENTS TO THE ACTO-MYO1B CROSS-BRIDGE

We designed a single molecule experiment in order to investigate the classical Huxley–Simmons (Huxley &

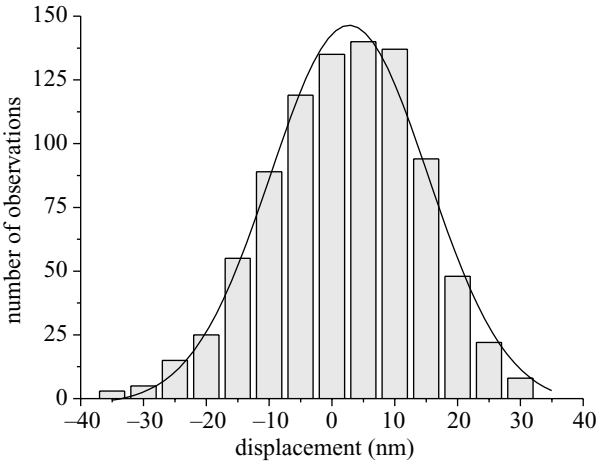

Figure 3. Frequency distribution of the amplitude of displacements. Individual event amplitudes were measured from the raw data relative to the actin filament rest position (see figure 2 for details). Amplitudes were binned into 5 nm bins. Measurements were obtained from seven separate filaments and results were pooled ($n = 827$). The fitted line is a Gaussian and the average displacement was 3.4 nm (see § 2c).

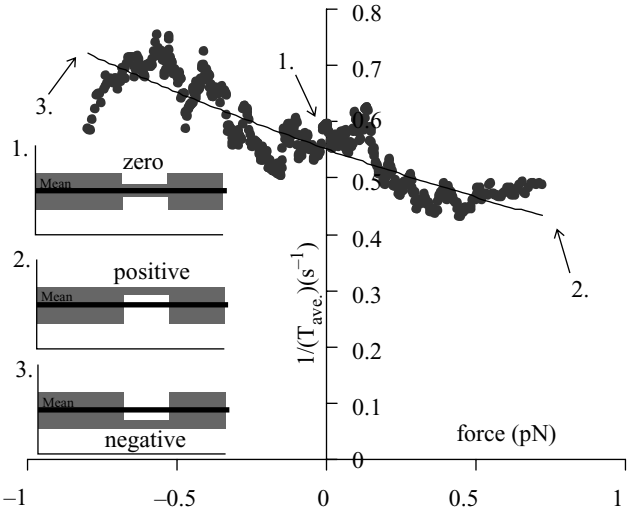

Figure 4. Scatter plot showing the load dependence of the average bound lifetimes. The lifetime of individual binding events was ranked on the basis of the applied force during the bound interval. The data (for both the timing and amplitude) was then averaged using a 40-point running average. The fitted line is an exponential fit. During the experiments, the actin filament moves due to thermal vibration, hence the load applied to the attached Myo1c cross-bridge during each event is quite variable. The load during some events is virtually zero, for others it is positive and others actually negative (see diagram inset). Data were collected at 20 μM ATP, pCa > 8, 23 °C.

Simmons 1971) T_2 behaviour of acto-Myo1b cross-bridges. Using a digital feedback loop (Molloy 1998) we controlled the position of the optically trapped beads and moved them with a triangular wave displacement of amplitude 25 nm peak-to-peak. The beads were moved at a frequency of 1 Hz. Our earlier studies (Veigel *et al.* 1999) indicated that these parameters would be of the correct size for us to observe tension fluctuations as the acto-Myo1b cross-bridge moved between structurally distinct bound conformations. The idea of the experiment and modelled response is shown in figure 5*a*,*b*. We expect to see sudden (vertical) transitions between parallel force–extension diagrams that correspond to movements between stable molecular conformations. The vertical separation of the force–extension diagrams is given by the product of cross-bridge stiffness κ_{xb} and distance between conformations, h. The horizontal separation of the lines is simply the distance, h.

If the rate constants governing the transition between states depend on load then one conformation should dominate at low (or negative) force and the other at high force. At intermediate loads one expects fluctuation between conformations to occur. This would be the region of inflexion of the T_2 curve measured for muscle fibres (Huxley & Simmons 1971). The T_2 behaviour of a single molecule will be different to an ensemble. Rather than a smooth inflexion in the force-extension diagram, occurring in the region of load where cross-bridges switch between states, we expect sudden vertical transitions (sudden changes in force) as the single cross-bridge rocks back or forth.

In our experiments, we applied a triangular wave oscillation to the beads holding the actin filament and then allowed Myo1b to interact with the actin. Because the bead position was under feedback control this signal followed the controlling triangular waveform faithfully (see figure 5*c*(ii)). However, the feedback signal sent to the acousto-optic modulators used to drive the tweezer position showed large and noisy excursions during the myosin attached intervals (figure 5*c*(ii)). From these records we calculated the force applied to the attached cross-bridge knowing the displacement of the bead from the tweezer centre and the tweezer stiffness. We then plotted the force applied against the measured bead position (figure 6). The resultant force–extension diagrams are non-linear. We believe the non-linearity arises from known non-linear series compliance in the system (Dupuis *et al.* 1997; Veigel *et al.* 1998). The records also showed regions in which the force–extension diagram was fairly smooth, interrupted by sudden stepwise changes in force (figure 6*b*, arrows) to a new, smooth force–extension plot (see figure 6*b*). In the current series of experiments we did not correct for series compliance. However, series compliance would not affect our estimate of the transition distance, h, derived from the force–extension diagrams.

We measured a total of 96 transitions (three examples are marked by arrows in figure 6*b*) from four actin filaments. The average estimate of the movement, h, associated with these transitions was 8.16 ± 0.13 nm (s.e.m.).

(a) *The nature of the Myo1c working stroke*

We found that Myo1c, like Myo1b (Veigel *et al.* 1999), produces its working stroke in at least two distinct phases. The first movement, of *ca* 3 nm, occurs within the time-resolution of our optical tweezers-based measurement and the second movement, of *ca* 1.5 nm, occurs after a delay of several milliseconds. We suggest that the first phase of the working stroke is produced as phosphate is released and that the second phase occurs as ADP is released from the acto-myosin bound complex (see figure 7).

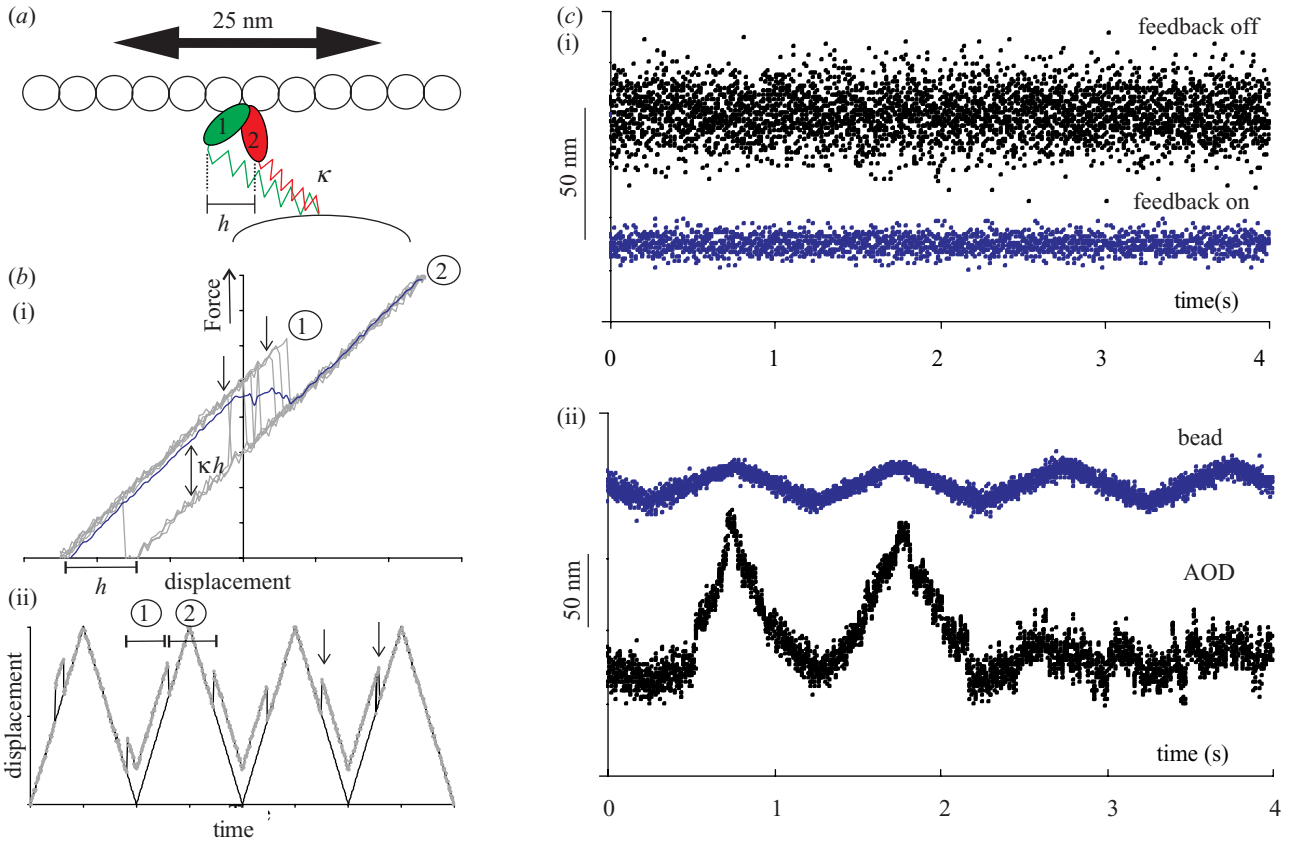

Figure 5. Application of controlled displacements to the acto-Myo1b cross-bridge. (*a*) A diagram showing how the traps move left and right applying forces to the myosin molecule. The red and green heads represent two different conformations that may occur when different directional forces are applied. (*b*) (ii) A model response. The black line represents the forcing function; the grey dots represent the position of the AOD. As the myosin head changes conformation transitions are observed in the data (marked 1 and 2). (i) The data from (ii) are plotted and a curve is obtained that shows the stiffness of the myosin cross-bridge and also clearly shows the transitions between state 1 and 2. The noise is adjusted deliberately to a low level for clarity. (*c*) (i) A plot comparing the position of a 1.1 μm bead held in the optical tweezers ($\kappa = 0.02$ pN nm^{-1}) when feedback is off (black) to when feedback in on (blue points). (ii) Using a digital feedback loop the beads are moved using a 25 nm peak-to-peak triangle wave (blue points). The feedback signal sent to the AOD, used to drive the bead position, shows large excursions during myosin-attached intervals.

The two-phase nature of the working stroke might act as a strain-sensitive mechanism that traps the cross-bridge in a bound, force-producing conformation (Cremo & Geeves 1998). If this idea is correct then only after the movement associated with ADP release occurs can the cross-bridge move forward to the rigor state, bind ATP and then detach from actin completing its catalytic cycle. This would mean that most acto-Myo1c molecules would populate in this force producing state and the system would therefore maintain tension very economically. Strong evidence for an ADP-induced, conformational change comes from the cryo-electron microscopy (Batters *et al.* 2004).

(b) *Myo1b rocks between different bound conformations*

We found that when Myo1b was subjected to a varying load the force–extension diagrams exhibited sudden, stepwise changes in force. We believe that these sudden changes in force result from actin-attached Myo1b molecules undergoing a conformational change that produces *ca* 0.3 pN of load (under the conditions of our experiments) corresponding to a movement of 8.16 nm. This movement is similar to the measured powerstroke for Myo1b (Veigel *et al.* 1999). We expect that Myo1c would show similar behaviour but that the movement produced would be less.

(c) *Weak binding states*

Myosin binding to actin is thought to be composed of three types of interactions: (i) an ionic interaction involving a flexible loop; (ii) a stereospecific interaction involving hydrophobic residues; and (iii) a strengthening of this by the recruitment of additional loops from the upper 50 kDa domain (Rayment *et al.* 1993). Several investigators have shown the existence of a 'weak binding' state in the acto-myosin cross-bridge cycle (see figure 7). During acto-S1 ATPase 10% of binding events result in ATP rather than ADP and Pi release (Sleep & Hutton 1978), suggesting a back detachment route, where no net hydrolysis of ATP takes place. The stiffness of single rabbit psoas fibres measured by application of rapid length changes was found to depend greatly upon the velocity of the length change. Very rapid filament sliding reveals a significant population of weakly bound myosin cross-bridges (Brenner *et al.* 1986). Finally, a single molecule mechanical study, using ATP analogues, where the hydrolytic step is rate limiting (Steffen *et al.* 2003) again revealed

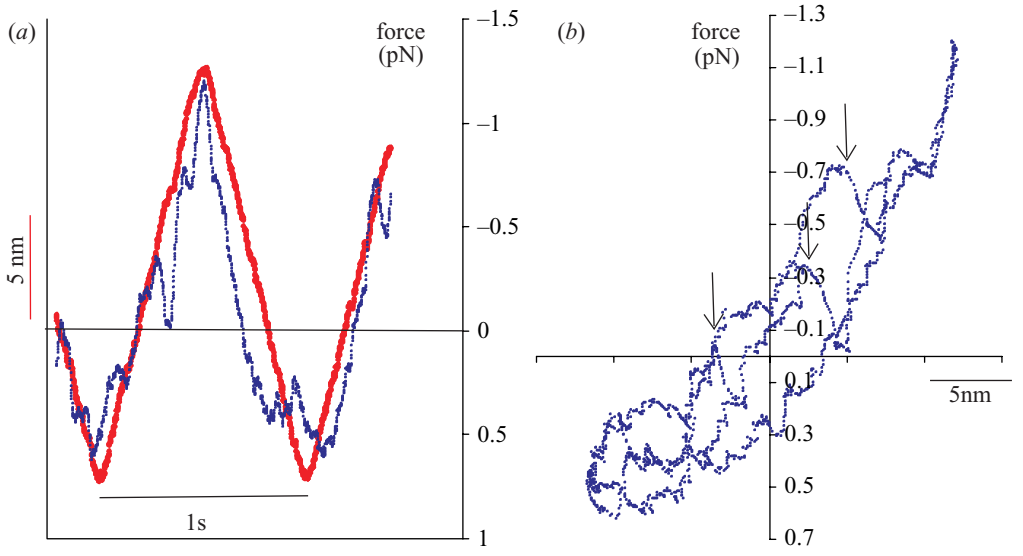

Figure 6. Force–extension diagrams for a single acto-Myo1b cross-bridge. (*a*) Trace showing the bead position (red) and the AOD position (blue). The trace is 2 s long and the myosin is bound to the actin for the duration. The red line demonstrates how well the bead follows the 25 nm triangle wave during binding interactions. A 50-point running average is applied to both the bead and AOD position data. (*b*) A force–displacement curve derived from (*a*).

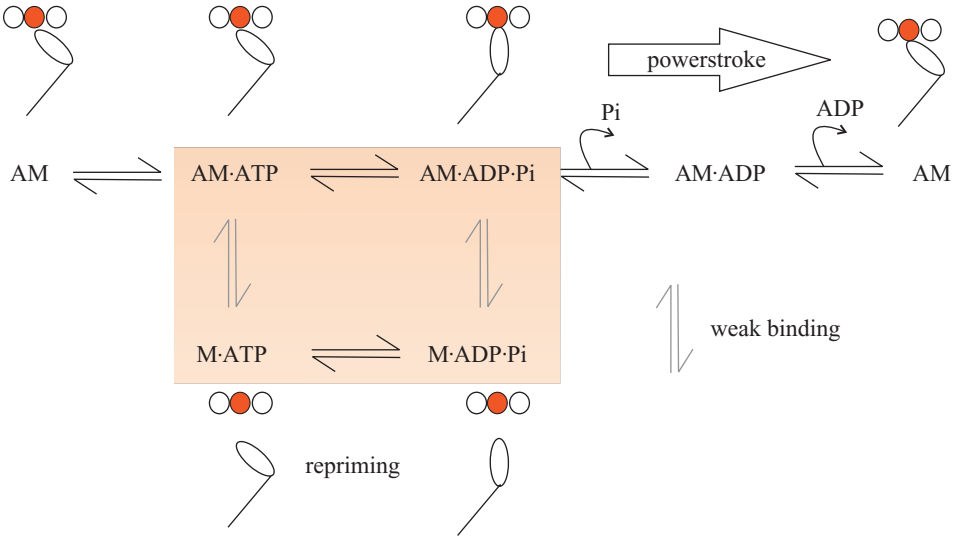

Figure 7. The acto-myosin cross-bridge cycle. The biochemical states are mapped onto the mechanical conformation of the myosin molecule. The shaded box encloses the weak-binding cross-bridge states.

an apparent zero-length working stroke due to binding and release of the weakly interacting, myosin products state.

Previous optical trapping studies, using both unconventional myosins and conventional rabbit skeletal myosin II, have failed to observe 'weak binding' states during the normal Mg·ATPase cycle. This is probably because the actin-attached and detached weak-binding states are in rapid equilibrium (e.g. the AM·ATP state dissociates to A+M·ATP very rapidly at *ca* 5000 s^{-1}; Trentham (1977)). The rates of association and dissociation are outside the time-resolution of the optical tweezer transducer apparatus; however, we show here and earlier (Batters *et al.* 2004) that the slow kinetics of Myo1c have enabled the weak-binding states to be observed directly at the single molecule level. Furthermore, unlike the weak-binding states of skeletal muscle fibres, we believe that those of Myo1c may have an important physiological role in the long-range 'slipping' adaptation process. The intermittent on/off binding interactions would produce a viscous interaction between the cluster of Myo1c molecules closely associated with the receptor ion channel.

(d) *Hair cell sensory mechanism*

(i) *Gating compliance explains early events in sensory physiology*

When stereocilia on hair cells are displaced laterally by a small amount (e.g. 100 nm), the bundles undergo a bending motion which produces shear between adjacent stereocilia. Tip-link filaments, which connect adjacent stereocilia, convert the shearing motion into a movement in plane with the plasma membrane of the taller stereocilium. The ratio of the tangential movement measured in

physiological experiments and the sliding motion in the plane of the membrane is *ca* 20 : 1 so a 100 nm displacement measured at the tip would produce a movement of *ca* 5 nm (Jacobs & Hudspeth 1990).

The tip-link filament is thought to form a stiff (Siemens *et al.* 2004; Sollner *et al.* 2004) connection with a mechanically-gated ion channel. The tip link serves two functions: it changes the geometry of the movements being sensed by the channel into the plane of the plasma membrane, and it converts the relatively large displacements but small forces associated with sound waves or head movements into small displacements and large forces. If we think about the energy involved in mechano-transduction: the work required to open an ion channel must be somewhat greater than thermal energy, k_BT (4 pN nm^{-1}), but probably less than 5 k_BT (20 pN nm^{-1}), which is the limit of sensitivity. Since the movement required to open an ion channel is the order of a nanometre (perhaps 2 nm) the force required to open it must be *ca* $20/2 = 10$ pN. It was found that stiffness of the stereocilia bundle is lower when deflected to a region at which channel opening occurs because work must be done to open the ion channel (Howard & Hudspeth 1988). This phenomenon, termed 'gating compliance', is a feature of the mechanism by which mechanical gating of the channel occurs. Because channel opening occurs within a few microseconds, the mechanical relaxation is too fast to resolve experimentally. Instead, the open probability remains at equilibrium with the mechanical load during the time-course of the stereocilia deflection. However, in all other respects the mechanical phenomenon is similar to the properties of single activated muscle fibres when subjected to a rapid mechanical perturbation. In fact, the mathematical analysis of Huxley & Simmons (1971) for such experiments, using suitable parameters, gives extremely good fits to the physiological data measured for hair cells.

We noticed that the adaptation process shows similar mechanical non-linearities to both the original gating events and also to muscle fibres. This leads to a new proposal: the adaptation process might be due to rearrangement of actin-bound Myo1c molecules and the slow return of the receptor potential arises not from many acto-Myo1c cycles (e.g. similar to steady-state muscle shortening) but instead is caused by movement produced while Myo1c is still bound to actin. Non-linearities in both the amplitude and rate of adaptation seen in published data seem correct for this class of model. If adaptation were due to a Myo1c conformational change then the process would be fast and complete for small deflections but slow and incomplete for large deflections of the stereocilia.

(ii) *Acto-myosin cross-bridge mechanism explains the slow adaptation process*

It is widely accepted that the non-linear mechanical and electrical properties of the hair cell, measured in response to small mechanical perturbations, results from the opening and closing of the ion channels (see § 1). What is more contentious is the mechanism responsible for the sensory adaptation process. Following a rapid bundle displacement, the hair cell receptor potential (which is a good measure of average tension in the tip-link filaments) gradually adapts towards the resting level. Channel closure presumably arises as tension in the tip-link connection is gradually relieved. The adaptation process is highly non-linear and cannot be explained by a simple, linear, mechanical system. For simplicity, in the models we develop below we have ignored the effects of the known gating compliance (discussed above) that would be in series with all of these models.

(iii) *Model A: a composite linear solid*

Our model consists of a spring with stiffness, κ_1, in series with a spring of stiffness κ_2 and dashpot (with viscous drag, c) combined in parallel (see figure 8*a*). When subjected to a step change in displacement, x_0, the force, F, at time, t, is given by:

$$F(t) = \frac{\kappa_2 x_0}{\kappa_1 + \kappa_2}\left[\kappa_1 + \kappa_2 \mathrm{e}^{\frac{(\kappa_1+\kappa_2)t}{c}}\right]. \tag{3.1}$$

The initial tension, T_1, and the final tension plateau, T_2, reached are linear functions of step size and the rate constant for tension recovery is independent of the displacement amplitude (figure 8*a*(iii) inset). This sort of model does not account for the adaptation process.

(iv) *Model B: a composite non-linear solid*

Our model consists of a nonlinear elastic element, for example, a biological polymer with WLC behaviour, in parallel with a dashpot both in series with a linear spring (figure 8*b*). Force in the WLC element is a non-linear function of its extension, x, and depends upon the polymer persistence length, L_P, contour length, L_0, and thermal energy, k_BT. A good approximation of this behaviour is given by Bustamante *et al.* (1994).

$$F = \frac{k_BT}{L_P}\left[\frac{1}{(1 - x/L_0)^2} - \frac{1}{4} + \frac{x}{L_0}\right]. \tag{3.2}$$

As the time dependence of this system is not simple, we determined the dynamic response of our composite non-linear solid using numerical methods. The response to a step change in length is linear in terms of T_1 but the final tension plateau, T_2, is highly non-linear and the rate constant is also non-linear. The tension recovery is virtually complete for small length changes but is incomplete for larger length changes. This is because the stiffness of the WLC element is low for small extensions but high for large extensions. This property is consistent with the amplitudes of receptor potential adaptation. However, non-linearity in the rate constant for tension recovery is of the opposite sense to that observed in hair cell adaptation. Force recovery is more rapid for large extensions than for small extensions. This is because higher system stiffness at large extension means that relaxation of the dashpot element is more rapid.

When subjected to a step change in displacement the initial tension, T_1, is a linear function of step amplitude; however, tension recovery, T_2, is now highly non-linear (figure 8*b*). Small displacements show almost full tension recovery whereas large displacements show incomplete recovery. This matches the amplitude behaviour of the sensory adaptation process well. However, the rate constant for tension (and therefore receptor potential)

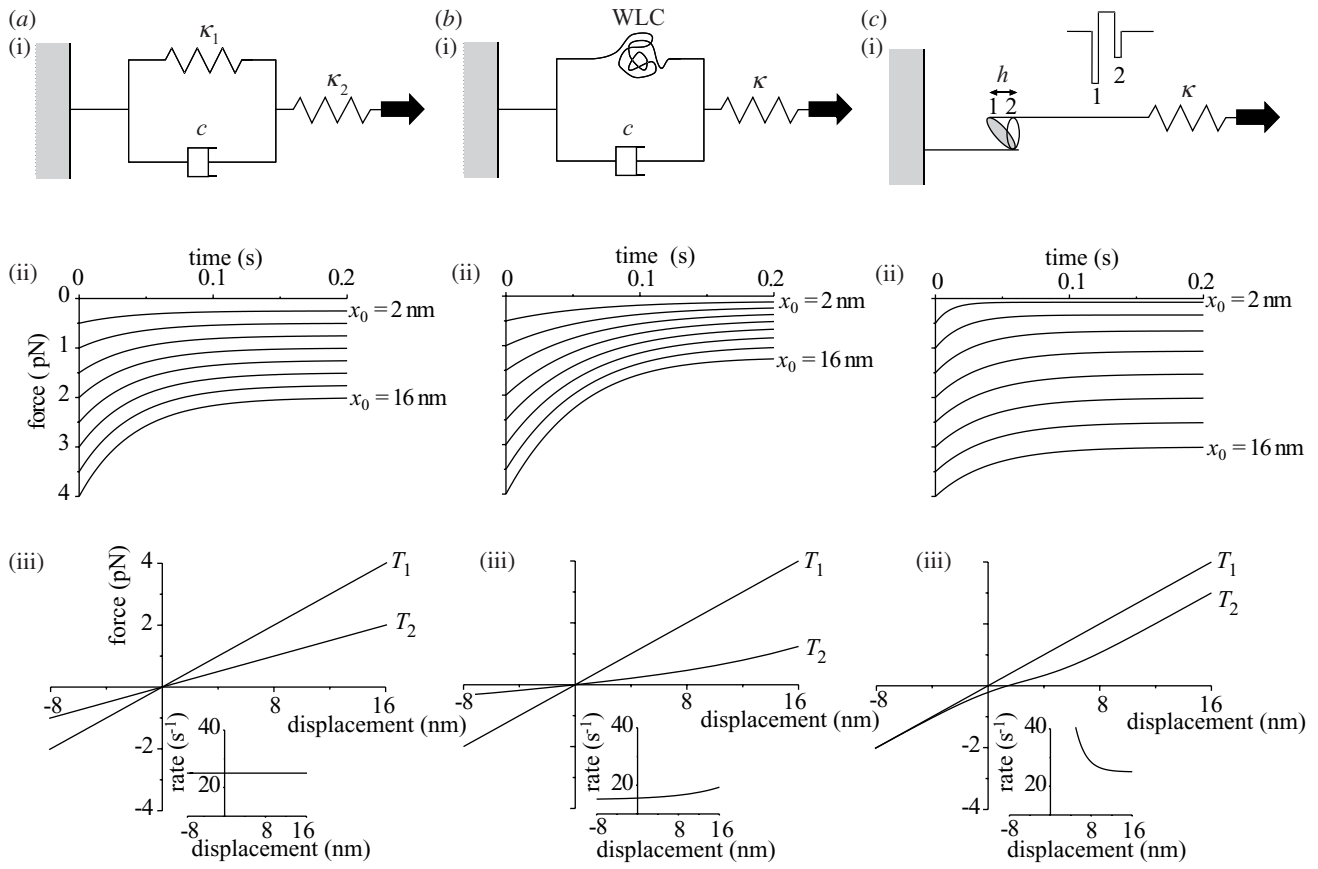

Figure 8. Three simple mechanical models for sensory adaptation. The mechanical models are shown in the diagrams (*a–c*) (i). A family of curves showing the time-course of force recovery following a step change in system length is shown in (*a–c*) (ii). The models were subjected to a sudden stretch (increase in length), the situation when a hair cell is deflected in the so-called positive direction (e.g. slipping adaptation). So that force–relaxation time courses can be compared directly with receptor potential plots, commonly presented in physiological studies of hair cell behaviour, the force scale is inverted. To highlight the key non-linearities in response of models B and C compared to model A, we have plotted the amplitude of the initial tension reached, T_1, the final tension plateau, T_2, and the rate constant for tension recovery, r, in (*a–c*)(iii). The inset in (*c*)(i) shows the relationship of the free energies of states 1 and 2. Length changes were over the range of $x_0 = 2$ to 16 nm in 2 nm steps; $\kappa_1 = \kappa_2 = \kappa = 0.25$ pN nm^{-1}; $c = 0.02$ pN nm s^{-1}; $k_B T = 4$ pN nm^{-1}; cross-bridge movement, $h = 4$ nm, $L_0 = 20$ nm, $L_p = 5$ nm. Note the shape of the T_2 curve in (*c*) is very sensitive to the chosen stiffness parameter, κ. If κ is increased (to 0.5 pN nm^{-1}) then characteristic overshoots of the T_2 curve occur (not shown here). Such overshoots have actually been measured for the ion channel gating process (Martin *et al.* 2000). If the phenomenon is also present within the adaptor motor apparatus then this might also contribute mechanical instability and be involved in mechanical amplification processes.

recovery becomes faster for larger displacements, the opposite of what is found. So again this simple model is insufficient to explain the physiological data.

(v) *Model C: a rocking cross-bridge model*

In our model, a single acto-Myo1c cross-bridge (or small cluster of bridges) is linked in series with a linear spring. In our analysis of the response of this system we have followed the treatment of Huxley & Simmons (1971). However, we do not assume that in the isometric state the population of the two states, n_1 and n_2, is equal. In fact, we assume a bias towards the angled state (state 1; see figure 8*c*). Tension recovery following a stretch occurs via those steeply angled cross-bridges (in state 1) rocking to a more upright position (state 2). In fact, the opposite bias might exist in muscle fibres since we know that the T_2 behaviour is much better characterized for muscle releases than for muscle stretches (the opposite for hair cell physiology).

The equilibrium constant, K_{eq}, relating to the population of the two states (n_1 and n_2), under no applied load is given by:

$$K_{eq} = \frac{n_1}{n_1 + n_2}. \tag{3.3}$$

Following the treatment of Huxley and Simmons, the forward, k_+, and backward, k_-, rates between the two states is given by:

$$k_+ = k_- \left(1 + K_{eq} e^{-\frac{\kappa h x}{k_B T}}\right). \tag{3.4}$$

Here, κ is the spring constant and h is the increase in length when the system shifts from state 1 to state 2. (In this section please note the similarity of the symbols for rate constants (k_+, k_-), equilibrium constant (K_{eq}), spring constant (κ) and Boltzmann's constant (k_B).)

Subsequently, the initial tension, T_1, and final tension, T_2, following an extension of amplitude, x, are:

$$T_1 = \kappa x, \tag{3.5}$$

$$T_2 = \kappa \left(\frac{K_{\mathrm{eq}} h}{4\mathrm{e}^{\frac{\kappa h x}{k_{\mathrm{B}} T}} + 2K_{\mathrm{eq}}} + x + x_{\mathrm{eq}} \right). \tag{3.6}$$

In our case, the extension of the link midway between the two states x_{eq} is assumed to be equal to half the distance between the two states, $x_{\mathrm{eq}} = -h/2$, i.e. T_2 is roughly zero for a displacement of $h/2$. This means that most cross-bridges are initially in state 1. In addition, the K_{eq} can be defined as:

$$K_{\mathrm{eq}} = \mathrm{e}^{\left(\frac{\kappa h^2}{2k_{\mathrm{B}} T}\right)}. \tag{3.7}$$

Following a length step of amplitude, x_0, the relaxation in force is given by:

$$F(t) = T_1 - (T_1 - T_2) \times \left(1 - \exp\left[-k_- \left(1 + K_{\mathrm{eq}} \mathrm{e}^{\frac{\kappa h x_0}{k_{\mathrm{B}} T}} \right) t \right] \right). \tag{3.8}$$

We find that, for the small signal case (*ca* 100 nm movement of the bundle tip), we do not need to invoke the idea that Myo1c slips along actin. Instead, tension recovery might occur via reversal of the myosin working stroke. Climbing adaptation could occur via the same mechanism. Larger displacements might require a greater degree of tension recovery. So, long-range adaptation may involve equilibration of the weak binding states of Myo1c during slipping adaptation and involve Myo1c taking several steps along the actin filament during climbing adaptation.

In our model, most of the attached bridges at equilibrium are in a near rigor state, ready to reverse their working stroke in response to ion-channel movement. From our optical trapping study, which showed a significant number of weak binding interactions, we believe there would be a significant pool of cross-bridges in weakly bound states. The total tension in the system is sufficient to hold the ion channels in a just closed position (open probability = 0.1).

Our model reproduces the correct behaviour in terms of the non-linearities in T_2 response and rate constant for force recovery. So the Huxley–Simmons theory, which assumes a load-dependent free energy barrier between two conformational states, can account for the small-signal behaviour observed for sensory adaptation of the hair cell receptor potential.

In summary, we find experimental evidence for a significant pool of weakly bound, Myo1c cross-bridges and a two-phase working stroke, giving *ca* 4 nm of movement. Using Myo1b we found that attached cross-bridges are able to move between different bound conformations in response to applied load. We expect that Myo1c will show the same properties. Movement produced by actin-attached Myo1c molecules at physiological calcium ion concentrations is probably sufficient to explain sensory adaptation. Furthermore, we believe that the adaptation process will depend critically upon the number of contributing myosins, their working stroke and their stiffness. Small differences in these parameters might explain the variable frequency of spontaneous mechanical oscillations (acoustic emissions) and proposed signal amplification by hair cells. Frequency tuning might be achieved by altering the number or effective stiffness of the myosins.

This work was supported by the Medical Research Council, UK, the IRC in Bionanotechnology, the NIH (GM 068080) and March of Dimes Birth Defect Foundation.

REFERENCES

Balish, M. F., Moeller, E. F. & Coluccio, L. M. 1999 Overlapping distribution of the 130- and 110-kDa myosin I isoforms on rat liver membranes. *Arch. Biochem. Biophys.* **370**, 285–293.

Batters, C., Arthur, C. P., Lin, A., Porter, J., Geeves, M. A., Milligan, R. A., Molloy, J. E. & Coluccio, L. M. 2004 Myo1c is designed for the adaptation response in the inner ear. *EMBO J.* **23**, 1433–1440.

Bose, A., Guilherme, A., Robida, S. I., Nicoloro, S. M. C., Zhou, Q. L., Jiang, Z. Y., Pomerleau, D. P. & Czech, M. P. 2002 Glucose transporter recycling in response to insulin is facilitated by myosin Myo1c. *Nature* **420**, 821–824.

Brenner, B., Chalovich, J. M., Greene, L. E., Eisenberg, E. & Schoenberg, M. 1986 Stiffness of skinned rabbit psoas fibers in MgATP and MgPPi solution. *Biophys. J.* **50**, 685–691.

Bustamante, C., Marko, J. F., Siggia, E. D. & Smith, S. 1994 Entropic elasticity of lambda-phage DNA. *Science* **265**, 1599–1600.

Coluccio, L. M. & Conaty, C. 1993 Myosin-I In mammalian liver. *Cell Motil. Cytoskel.* **24**, 189–199.

Coluccio, L. R. & Geeves, M. A. 1999 Transient kinetic analysis of the 130-kDa myosin I (MYR-1 gene product) from rat liver—a myosin I designed for maintenance of tension? *J. Biol. Chem.* **130**, 21 575–21 580.

Cordonnier, M. N., Dauzonne, D., Louvard, D. & Coudrier, E. 2001 Actin filaments and myosin I alpha cooperate with microtubules for the movement of lysosomes. *Mol. Biol. Cell* **12**, 4013–4029.

Corey, D. P. & Hudspeth, A. J. 1983 Analysis of the microphonic potential of the bullfrogs sacculus. *J. Neurosci.* **3**, 942–961.

Cremo, C. R. & Geeves, M. A. 1998 Interactions of actin with ADP with the head domain of smooth muscle myosin: implications for strain-dependent ADP release in smooth muscle. *Biochemistry* **37**, 1969–1978.

Diefenbach, T. J., Latham, V. A., Yimlamai, D., Liu, C. A., Herman, I. M. & Jay, D. G. 2002 Myosin 1c and myosin IIB serve opposing roles in lamellipodial dynamics of the neuronal growth cone. *J. Cell Biol.* **158**, 1207–1217.

Dupuis, D. E., Guilford, W. H., Wu, J. & Warshaw, D. M. 1997 Actin filament mechanics in the laser trap. *J. Muscle Res. Cell Motil.* **18**, 17–30.

Finer, J. T., Simmons, R. M. & Spudich, J. A. 1994 Single myosin molecule mechanics: piconewton forces and nanometre steps. *Nature* **368**, 113–118.

Garcia, J. A., Yee, A. G., Gillespie, P. G. & Corey, D. P. 1998 Localization of myosin-1 beta near both ends of tip links in frog saccular hair cells. *J. Neurosci.* **18**, 8637–8647.

Gillespie, P. G. 2004 Myosin-I and adaptation of mechanical transduction by the inner ear. *Phil. Trans. R. Soc. B* **359**. 1945–1951. (doi:10.1098/rstb.2004.1564.)

Gillespie, P. G. (and 27 others) 2001 Myosin-I nomenclature. *J. Cell Biol.* **155**, 703–704.

Gillespie, P. G., Wagner, M. C. & Hudspeth, A. J. 1993 Identification of a 120 Kd hair-bundle myosin located near stereociliary tips. *Neuron* **11**, 581–594.

Glowatzki, E. & Fuchs, P. A. 2002 Transmitter release at the hair cell ribbon synapse. *Nature Neurosci.* **5**, 147–154.

Holt, J. R. & Corey, D. P. 2000 Two mechanisms for transducer adaptation in vertebrate hair cells. *Proc. Natl Acad. Sci. USA* **97**, 11 730–11 735.

Holt, J. R., Gillespie, S. K., Provance, D. W., Shah, K., Shokat, K. M., Corey, D. P., Mercer, J. A. & Gillespie, P. G. 2002 A chemical-genetic strategy implicates myosin-1c in adaptation by hair cells. *Cell* **108**, 371–381.

Howard, J. & Hudspeth, A. J. 1987 Mechanical relaxation of the hair bundle mediates adaptation in mechanoelectrical transduction by the bullfrogs saccular hair cell. *Proc. Natl Acad. Sci. USA* **84**, 3064–3068.

Howard, J. & Hudspeth, A. J. 1988 Compliance of the hair bundle associated with gating of mechanoelectrical transduction channels in the bullfrogs saccular hair cell. *Neuron* **1**, 189–199.

Huxley, A. F. & Simmons, R. M. 1971 Proposed mechanism of force generation in muscle. *Nature* **233**, 533–538.

Jacobs, R. A. & Hudspeth, A. J. 1990 Ultrastructural correlates of mechanoelectrical transduction in hair cells of the bullfrogs internal ear. *Cold Spring Harbor Symp. Quant. Biol.* **55**, 547–561.

Kishino, A. & Yanagida, T. 1988 Force measurements by micromanipulation of a single actin filament by glass needles. *Nature* **334**, 74–76.

Kron, S. J. & Spudich, J. A. 1986 Fluorescent actin filaments move on myosin fixed to a glass surface. *Proc. Natl Acad. Sci. USA* **83**, 6272–6276.

Kros, C. J., Marcotti, W., van Netten, S. M., Self, T. J., Libby, R. T., Brown, S. D. M., Richardson, G. P. & Steel, K. P. 2002 Reduced climbing and increased slipping adaptation in cochlear hair cells of mice with Myo7a mutations. *Nature Neurosci.* **5**, 41–47.

Marquis, R. E. & Hudspeth, A. J. 1997 Effects of extracellular Ca2+ concentration on hair-bundle stiffness and gating-spring integrity in hair cells. *Proc. Natl Acad. Sci. USA* **94**, 11 923–11 928.

Martin, P., Mehta, A. D. & Hudspeth, A. J. 2000 Negative hair-bundle stiffness betrays a mechanism for mechanical amplification by the hair cell. *Proc. Natl Acad. Sci. USA* **97**, 12 026–12 031.

Molloy, J. E. 1998 Optical chopsticks: digital synthesis of multiple optical traps. *Meth. Cell Biol.* **55**, 205–216.

Molloy, J. E., Burns, J. E., Kendrick Jones, J., Tregear, R. T. & White, D. C. S. 1995 Movement and force produced by a single myosin head. *Nature* **378**, 209–212.

Pardee, J. D. & Spudich, J. A. 1982 Purification of muscle actin *Meth. Enzymol.* **85**, 164–181.

Rayment, I., Rypniewski, W. R., Schmidtbase, K., Smith, R., Tomchick, D. R., Benning, M. M., Winkelmann, D. A., Wesenberg, G. & Holden, H. M. 1993 Three-dimensional structure of myosin subfragment-1—a molecular motor. *Science* **261**, 50–58.

Ruppert, C., Kroschewski, R. & Bahler, M. 1993 Identification, characterization and cloning of Myr-1, a mammalian myosin-I. *J. Cell Biol.* **120**, 1393–1403.

Siemens, J., Lillo, C., Dumont, R. A., Reynolds, A., Williams, D. S., Gillespie, P. G. & Muller, U. 2004 Cadherin 23 is a component of the tip link in hair cell stereocilia. *Nature* **428**, 950–955.

Sleep, J. A. & Hutton, R. L. 1978 Actin mediated release of ATP from a myosin-ATP complex. *Biochemistry* **17**, 5423–5430.

Sollner, C., Rauch, G. J., Siemens, J., Geisler, R., Schuster, S. C., Tubingen 2000 Screen Consortium, t., Muller, U. & Nicolson, T. 2004 Mutations in cadherin 23 affect tip links in zebrafish sensory hair cells. *Nature* **428**, 955–959.

Steffen, W., Smith, D. & Sleep, J. 2003 The working stroke upon myosin-nucleotide complexes binding to actin. *Proc. Natl Acad. Sci. USA* **100**, 6434–6439.

Tang, N. Y., Lin, T. M. & Ostap, E. M. 2002 Dynamics of Myo1c (myosin-I beta) lipid binding and dissociation. *J. Biol. Chem.* **277**, 42 763–42 768.

Trentham, D. R. 1977 The ATPase reactions of myosin and actomyosin and their relation to energy transduction in muscle *Biochem. J.* **5**, 5–22.

Veigel, C., Bartoo, M. L., White, D. C. S., Sparrow, J. C. & Molloy, J. E. 1998 The stiffness of rabbit skeletal actomyosin cross-bridges determined with an optical tweezers transducer *Biophys. J.* **75**, 1424–1438.

Veigel, C., Coluccio, L. M., Jontes, J. D., Sparrow, J. C., Milligan, R. A. & Molloy, J. E. 1999 The motor protein myosin-I produces its working stroke in two steps. *Nature* **398**, 530–533.

Weil, D., Blanchard, S., Kaplan, J., Guilford, P., Gibson, F., Walsh, J., Mburu, P., Valera, A., Levillers, J. & Weston, M. D. 1995 Defective myosin VIIA gene responsible for usher syndrome typeB. *Nature* **374**, 60–61.

Wu, Y. C., Ricci, A. J. & Fettiplace, R. 1999 Two components of transducer adaptation in auditory hair cells. *J. Neurophysiol.* **82**, 2171–2181.

GLOSSARY

AOD: acousto-optic deflector
WLC: worm-like chain
NEM: *N*-ethyl maleimide